LIMNOLOGY and OCEANOGRAPHY

ASLO

Limnol. Oceanogr. 9999, 2021, 1–14

doi: 10.1002/lno.11922

The redox fate of hydrogen peroxide in the marine water column

Kevin M. Sutherland,[1,2,3] **Kalina C. Grabb**,[1,2] **Jennifer S. Karolewski**,[1,2] **Lina Taenzer**,[1,2] **Colleen M. Hansel**,[1] **Scott D. Wankel**[1*]

[1]Department of Marine Chemistry and Geochemistry, Woods Hole Oceanographic Institution, Woods Hole, Massachusetts
[2]Department of Earth, Atmospheric and Planetary Science, Massachusetts Institute of Technology, Cambridge, Massachusetts
[3]Department of Earth and Planetary Science, Harvard University, Cambridge, Massachusetts

Abstract

Marine microbes produce extracellular reactive oxygen species (ROS) such as superoxide and hydrogen peroxide (H_2O_2) as a result of regulated and nonregulated physiological and metabolic reactions. ROS production can be a sink and cryptic recycling flux of dissolved oxygen that may rival other key fluxes in the global oxygen cycle; however, the low abundance and high turnover rate of ROS makes this figure difficult to constrain. One key step in determining the disparity between the gross production of ROS and the net sink of dissolved oxygen lies in understanding the degradation pathways of H_2O_2 in the marine water column. In this study, we use isotope-labeling techniques to determine the redox fate of H_2O_2 in a range of marine environments off the West Coast of California. We find that H_2O_2 reduction is greater than or equal to H_2O_2 oxidation at most sampled depths, with notable exceptions in some surface and intermediate water depths. The observation that H_2O_2 oxidation can exceed reduction in the dark ocean indicates the presence of an oxidizing decay pathway that is not among the known suite of microbially mediated enzymatic pathways (i.e., catalase and peroxidase), pointing to an abiotic and/or a nonenzymatic decay pathway at intermediate water depths. These results highlight the complexity and heterogeneity of ROS decay pathways in natural waters and their unconstrained regulation of oxygen levels within the ocean.

Reactive oxygen species (ROS), as the name implies, are short-lived, reactive, oxygen-containing molecules that have lifetimes in aquatic systems ranging from less than a second to days. Common ROS in marine environments include hydrogen peroxide (H_2O_2), superoxide ($O_2^{\bullet-}/HO_2$), and hydroxyl radical ($HO^{\bullet}$), which are typically found at picomolar to nanomolar levels. Many ROS in seawater ultimately stem from univalent reduction of O_2, a diradical with two unpaired electrons in parallel spin, to $O_2^{\bullet-}$ (Fridovich 1998). Superoxide and H_2O_2 are pervasive in the global ocean, mediating a wide range of surface redox reactions, including the oxidation and remineralization of simple and complex organic compounds, and oxidation and reduction of essential nutrients and terminal electron acceptors (Rose et al. 2008; Wuttig et al. 2013).

The origins of and relationship between $O_2^{\bullet-}$ and H_2O_2 are complex. For example, light absorption by colored dissolved organic matter (CDOM) in sunlit surface waters will induce an electron transfer to dissolved oxygen, producing $O_2^{\bullet-}$ (Zhang et al. 2012). In the marine environment, $O_2^{\bullet-}$ may serve as an oxidant or a reductant depending on the nature of the reactant species and the particular environmental conditions (Powers and Miller 2015). The net result is that $O_2^{\bullet-}$ is either oxidized back to O_2 or reduced to H_2O_2. Superoxide will often undergo catalyzed or uncatalyzed dismutation, in which both O_2 and H_2O_2 result as products. Superoxide reduction is thought to be the primary pathway through which H_2O_2 is formed (Zhang et al. 2012). However, reports of H_2O_2 production rates exceeding those of $O_2^{\bullet-}$ production (Zhang et al. 2016), or of $O_2^{\bullet-}$ production rates exceeding the 2 : 1 stoichiometry expected for dismutation (Powers et al. 2015) suggest a more complex series of operative formation pathways and the potential decoupling of these two ROS.

Photochemical processes do not have a monopoly on the production of ROS in natural waters. Light-independent microbial ROS production is widespread in the surface and deep ocean (Palenik and Morel 1988; Roe et al. 2016; Hopwood et al. 2017). In some cases, dark ROS production even rivals that of photochemical production (Vermilyea et al. 2010; Roe et al. 2016). Marine microbes in the photic and aphotic zone alike are significant sources of the ROS $O_2^{\bullet-}$, and therefore H_2O_2 (Sutherland et al. 2019). Dark, particle-associated $O_2^{\bullet-}$ and H_2O_2 have been observed in both freshwater and seawater, and have been found to result directly

*Correspondence: sdwankel@whoi.edu

Additional Supporting Information may be found in the online version of this article.

from the presence of living cells (Roe et al. 2016; Zhang et al. 2016; Sutherland et al. 2020*a*).

Light-independent ROS production can be incidental or linked to organismal physiological and metabolic activity (Hansel and Diaz 2021). Several metabolic reactions, including aerobic respiration, photosynthesis, and photorespiration, produce $O_2^{\bullet -}$ and H_2O_2 as a byproduct with no apparent benefit. Excess buildup of these ROS inside the cell is a state commonly referred to as "oxidative stress," which can degrade cell health, damage cell machinery, and lead to cell death (Ryter et al. 2007; Sheng et al. 2014). Mediated ROS production, however, plays a critical role to cell health. H_2O_2 specifically plays a role in many cell signal transduction pathways, differentiation, proliferation, and innate immune response (Zamocky et al. 2008; Lennicke et al. 2015).

The presence of ROS in sunlit and dark natural waters has far-reaching implications for dissolved oxygen in the environment. Intracellular ROS have been recognized for decades for their role as a significant global sink of oxygen (Mehler 1951; Guy et al. 1993; Bender et al. 1994). Mehler photoreduction of O_2 can comprise > 40% of total electron flow in some cyanobacteria (Kana 1993; Helman 2005). A recent study suggests that extracellular ROS may also be an important sink in the global oxygen cycle, accounting for an estimated 5% to 20% of net oxygen consumption in the marine biosphere (Sutherland et al. 2020*b*). An important source of uncertainty in constraining the amount of oxygen that ultimately results from extracellular $O_2^{\bullet -}$ production and degradation, however, lies in the redox fate of H_2O_2. Further review of the underlying assumptions of the fate of H_2O_2 is critical to better constraining the role of ROS in the global oxygen and carbon budgets.

Microbes, in addition to being prolific sources of ROS to the marine water column, are also the primary sink of H_2O_2 in natural water. Studies of freshwater and seawater have shown that filtration and/or sterilization of natural waters nearly eliminates its H_2O_2 degrading activity (Cooper and Zepp 1990; Moffett and Zafiriou 1990). Although abiotic factors such as sunlight and metal concentrations can influence the H_2O_2 decay rate in natural waters, one study demonstrated that photochemical H_2O_2 decay rates are at most 5% of dark, particle-mediated peroxide degradation (Moffett and Zafiriou 1993). Microbial communities are typically equipped with two classes of enzymes for degrading H_2O_2: catalases and peroxidases. These two enzyme classes having the following stoichiometry:

$$2H_2O_2 \longrightarrow 2H_2O + O_2 \text{ (Catalase)}, \quad (1)$$

$$H_2O_2 + AH_2 \longrightarrow 2H_2O + A \text{ (Peroxidase)}. \quad (2)$$

The stoichiometries of catalase- and peroxidase-mediated H_2O_2 decay set practical boundaries for the oxidation–reduction ratios of H_2O_2 for natural marine waters. In the case of catalase-mediated disproportionation, 50% of the oxygen in H_2O_2 is reduced to H_2O and eliminated from the O_2 pool, while the remaining 50% is re-oxidized back to O_2. Peroxidase-mediated H_2O_2 degradation will result in the complete reduction of H_2O_2 to water concomitant with the oxidation of an electron donor. It is important to note that catalases and peroxidases comprise diverse enzyme families with a wide range of cofactors and substrates and include bifunctional members that can exhibit catalase and peroxidase stoichiometry (Zamocky et al. 2008). All references to catalase and peroxidase in this study refer to the stoichiometries and not any particular enzyme.

The relative activity of these two classes of enzymes is, in part, a reflection of the activity of the microbial consortium present in a water mass at a given time. Many ubiquitous marine microbes do not contain known genes encoding for catalase (e.g., *Prochlorococcus*, Thaumarchaeota) (Morris et al. 2011; Hollibaugh 2017). These microorganisms may rely on a combination of peroxidase activity and nearby catalase-containing microbes to manage H_2O_2 levels (Morris et al. 2011). Therefore, the microbial community, their H_2O_2-metabolizing enzyme expression, and the relative activity of these enzymes will all interact to determine the fraction of oxygen cycled through ROS pathways that is ultimately reduced to water—thereby governing the ROS-mediated O_2 sink. Dissolved oxygen reduction via ROS pathways can thus influence the availability of an important electron acceptor and decrease the overall energy yield of oxygen utilization by microorganisms. One previous study used an isotope-labeling approach to characterize the relative redox fate of H_2O_2 in one productive surface ocean setting (Moffett and Zafiriou 1990). The authors determined that 65% to 80% of H_2O_2 decay resulted from catalase-like stoichiometry, with the remainder resulting from peroxidase-like stoichiometry.

Here, we build upon this previous work to determine the redox fate of H_2O_2 under a wide range of environmental conditions off the West Coast of California in the Northeast Pacific Ocean. Using a novel isotope-labeling technique, we investigate the dark decomposition of H_2O_2 at depths ranging from the surface to 3000 m and oxygen concentrations ranging from supersaturation down to tens of $\mu mol\ kg^{-1}$ O_2. In performing this set of measurements, we set out to determine the extent to which H_2O_2 production, and ROS cycling more generally, contributes to the net consumption of oxygen.

Methods

Sample collection

Seawater samples used in H_2O_2 incubations were collected aboard the *R/V Atlantis* in October 2019. Samples were collected at three stations along the California Coast. Sta. 1 (latitude: 35.750, longitude: −122.599) was located off the continental shelf, just east of Davidson Seamount (Fig. 1). Water samples at Sta. 1 were collected from six depths ranging

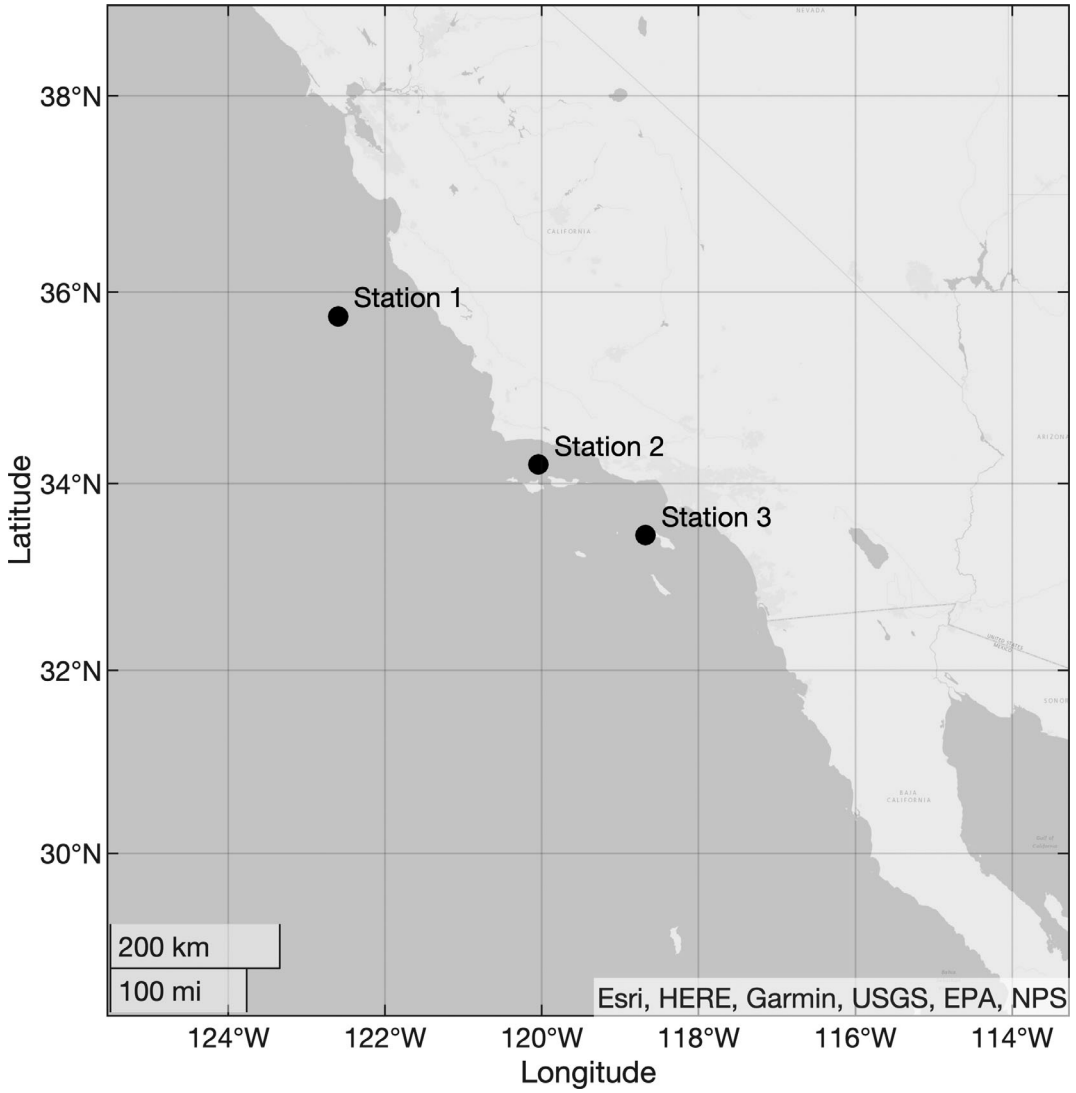

Fig 1. Location of the stations sampled in this study.

from 4 to 3000 m beneath the surface. Sample collection began at approximately 4 a.m. local time. Sample depths were chosen based on conductivity, temperature and depth (CTD) dissolved oxygen readings to ensure that the sample depths covered the overall structure of the dissolved oxygen profile. Sta. 2 (latitude: 34.200, longitude: −120.041) was located in the Santa Barbara Basins (Fig. 1), a dysoxic marine environment that is characterized by exceptionally low oxygen concentrations at depth, and nanomolar dissolved sulfide concentrations beneath the photic zone (Kuwabara et al. 1999). Waters in the Santa Barbara Basin can be subject to periodic flushing with more oxygen-rich waters; however, this did not appear to be the case at the time of sampling (Bograd et al. 2002). Samples were collected at five depths along a monotonic decrease in dissolved oxygen with depth, ranging from 5 to 350 m beneath the surface. Sample collection began at approximately 10 : 30 a.m. local time. Sta. 3 (latitude: 33.452, longitude: −118.677) was located within view of Catalina Island (Fig. 1), and meant to provide a much higher resolution sampling of waters in the photic zone. Sta. 3 was sampled at five depths ranging from 5 to 40 m beneath the surface. Sample collection began at approximately 7 p.m. local time (just after sunset).

Samples were collected using Niskin bottles affixed to a stainless-steel rosette equipped with a CTD. Niskin bottles were acid cleaned, soaked in local seawater, and rinsed thoroughly prior to deployment. Water was transferred directly from the Niskin bottle into a polyethylene collapsible container, taking care to minimize agitation at the water surface and avoid incidental gas exchange. Water was amended and prepared for incubations as described below. While some previous studies have used a trace metal clean rosette for

collection and analysis of H_2O_2, two previous studies have found the overall influence of nontrace-metal clean seawater sampling acceptable for analysis of H_2O_2 (Rose et al. 2010; Hopwood et al. 2017). Hopwood et al. (2017) in a direct comparison of trace-metal clean sampling methods and traditional Niskin sampling methods found that samples from a traditional Niskin were higher by approximately 1 nM, well below the analytical precision reported in our present study and well below the 500 nM H_2O_2 spike we describe below. All other sampling equipment and incubation bottles were acid washed with 10% HCl (prepared with 18.2 MΩ water) for a minimum of 24 h.

Isotope labeling

H_2O_2 oxidation rate, reduction rate, and, in their sum, gross decay rate were determined with the addition of 500 nM of isotopically labeled H_2O_2 prepared with $H_2{}^{17}O_2$ (> 90% ^{17}O, ICON Isotopes/Berry and Associates). This amendment is ~ 3–6 times a typical midday H_2O_2 concentration in sunlit surface water, and several hundred times a typical deep ocean H_2O_2 concentration (Hopwood et al. 2017). This method is very similar to those described in Moffett and Zafiriou (1990) with a few modifications. In short, we monitored the change in labeled H_2O_2 over time and the evolution of the doubly substituted $^{34}O_2$ isotope label into the dissolved oxygen pool, using mass balance to constrain the total oxidative and reductive sinks of H_2O_2. A solution of $H_2{}^{17}O_2$ (Berry and Associates/ICON Isotopes) was diluted with 3% H_2O_2 (Sigma) and ultrapure water. The spike was added to several liters of sample, homogenized in a collapsible volume without headspace to minimize gas exchange, and aliquoted into 125-mL Wheaton serum vials. The bottles were capped and crimped with no headspace and incubated in the dark for between 12 and 48 h. A temperature-controlled room was used to keep samples as close as possible to the temperature at which they were collected. The temperature-controlled room was set to between 4°C and 12°C, determined by the average temperature of samples collected below the thermocline. Samples collected above the thermocline were incubated in the cold room or at ambient lab temperature, whichever was closer to the collection temperature.

Incubations consisted of between 3 and 6 timepoints over the incubation period. At each time point, four biological replicate bottles were sacrificed and sampled using one of two treatments. In the first treatment (Treatment 1), dissolved oxygen was extracted to monitor the evolution of $^{34}O_2$ (^{17}O—^{17}O) into the dissolved oxygen pool. Dissolved oxygen was collected from the sample by adding a 5 mL headspace of ultrahigh-purity helium gas, and equilibrating by rapidly shaking the sample on an orbital shaker for at least 30 min. We tested the effect of equilibration times as long as 48 h and found no significant difference in O_2 isotope composition of labeled samples or O_2 : Ar ratio when samples were equilibrated for longer. The headspace gas was collected from each bottle using a Hamilton Sample Lock syringe and transferred to a He-flushed 2-mL serum vial. This over-pressurized mixture of He and sample gas was found to have high fidelity against atmospheric contamination as no measurable change was observed in a labeled standard over the period of collection and analysis. In the second treatment (Treatment 2), all remaining labeled H_2O_2 was oxidized to O_2 to monitor the decline of label in the O_2 (sum of natural oxidation and the H_2O_2 transformed by the oxidizing treatment) over time, which was inferred to result from H_2O_2 reduction. In this treatment, samples were amended with 1 mL of potassium permanganate ($KMnO_4$) slurry (40 mg mL^{-1}) and acidified with 100 μL 6 N hydrochloric acid (HCl) to rapidly oxidize all remaining labeled H_2O_2 to O_2 gas (Savarino and Thiemens 1999). The oxygen collected from Treatment 2 contains the combined label (now as O_2) from both natural H_2O_2 oxidation and the unreacted H_2O_2. The amount of H_2O_2 that was reduced to water (or other reductive pathways) was calculated by difference.

The oxygen isotope composition and O_2 : Ar were measured on an Isoprime100 isotope ratio mass spectrometer modified with a manual injection port as previously described (Long et al. 2020). O_2 : Ar ratios were used to determine the extent to which O_2 was consumed by dark cellular processes over the course of the incubation. $H_2^{17}O_2$ was chosen instead of $H_2^{18}O_2$ because biological H_2O_2 oxidation to O_2 proceeds via a nonscrambling mechanism, meaning the oxygen—oxygen bond in H_2O_2 is preserved during oxidation (Vlasits et al. 2007). The resulting ^{17}O—^{17}O molecule can be analyzed in the same manner that traditional ^{18}O measurements are collected (as mass/charge 34) (e.g., Wassenaar et al. 2010). H_2O_2 decay in natural waters follows pseudo-first-order kinetics (Moffett and Zafiriou 1990), meaning we can apply the following set of equations to determine the decay rate constants for oxidation, reduction, and total H_2O_2 loss:

$$^{34}R_{\text{sample}} = \frac{^{34}O_2}{^{32}O_2}, \tag{3}$$

$$X_{\text{label}} = \frac{^{34}R_{\text{sample}}}{^{34}R_{KMnO_4,t=0}}, \tag{4}$$

$$\left[\frac{d[H_2O_2{}^*]}{dt}\right]_{\text{oxidation}} = -k_{\text{ox}}\left[1 - \left(X_{\text{label}}(t)_{\text{Treatment 1}}\right)\right], \tag{5}$$

$$ln\left(1 - \left(X_{\text{label}}(t)_{\text{Treatment 1}}\right)\right) = -k_{\text{ox}}t, \tag{6}$$

$$\left[\frac{d[H_2O_2{}^*]}{dt}\right]_{\text{reduction}} = -k_{\text{red}}\left[X_{\text{label}}(t)_{\text{Treatment2}}\right], \tag{7}$$

$$ln(X_{\text{label}}(t)_{\text{Treatment 2}}) = -k_{\text{red}}t, \quad (8)$$

$$k_{\text{loss}} = k_{ox} + k_{\text{red}}, \quad (9)$$

where ^{34}R represents the ratio of $^{34}O_2$ to $^{32}O_2$, X_{label} represents the fraction of the starting H_2O_2 label that is present in the dissolved O_2 pool in either Treatment 1 (monitoring for oxidative decay) or Treatment 2 (monitoring for reductive decay), t represents time (in hours), and k represents the decay rate constant with respect to oxidation, reduction, or both. The values of k_{ox}, k_{red}, and their respective uncertainties were determined using a linear fit on the log-transformed data vs. time using the polyfit function in MATLAB. All uncertainties of derived values were propagated in their entireties (e.g., k_{loss} uncertainty contains propagated uncertainty of both k_{ox} and k_{red}). An example of the incubation data is shown in Fig. 2.

The 500 nM spike of $H_2^{17}O_2$ was prepared such that the mass 34 contribution to the O_2 pool would be sufficiently high to resolve H_2O_2 decay at the percent level. Specifically, the $^{34}O_2$: $^{32}O_2$ of the spike was ~0.15, which, when completely oxidized to the O_2 pool (~1 in 300 dilution for water in equilibrium with atmosphere) yielded a "$\delta^{18}O$ equivalent" of ~100–200 permil. Multiple quality control measures were taken to ensure high-quality data. Process blanks were conducted in which 18.2 MΩcm was treated as a sample and run through the steps of preparation and incubation, including one that ran for twice as long as the longest incubation in this study. In all cases, no label was observed to decay within the precision of the mass spectrometer (~1% of label). The O_2 : Ar ratio in all cases was sufficiently different from air that it can be used as a tracer of sample contamination. In cases where the biological replicates exhibited a difference in O_2 : Ar of more than 5%, the sample that had an O_2 : Ar ratio closer to air was rejected from the sample set (rejected 3 of the approximately 450 individual samples collected). For each incubation, four bottles of seawater were collected and incubated without the addition of the isotope label to monitor background changes in O_2 : Ar and $^{34}O_2$ arising from microbial oxygen utilization. Oxygen utilization in most samples ranged from undetectable to 1.5%; however, one sample in the surface water of Sta. 3 saw 2.5% decrease in dissolved oxygen. The corresponding increases in the relative abundance of $^{34}O_2$ arising from kinetic isotope effects associated with respiration and other microbial processes were negligible. All analyses were conducted within 4 months of collection.

Field H_2O_2 quantification

All rates presented in this study were determined using the isotopically labeled H_2O_2, as outlined above. In addition, real-time H_2O_2 concentration measurements were conducted to monitor decay of the H_2O_2 spike for the purpose of determining the appropriate experiment duration. H_2O_2 concentrations

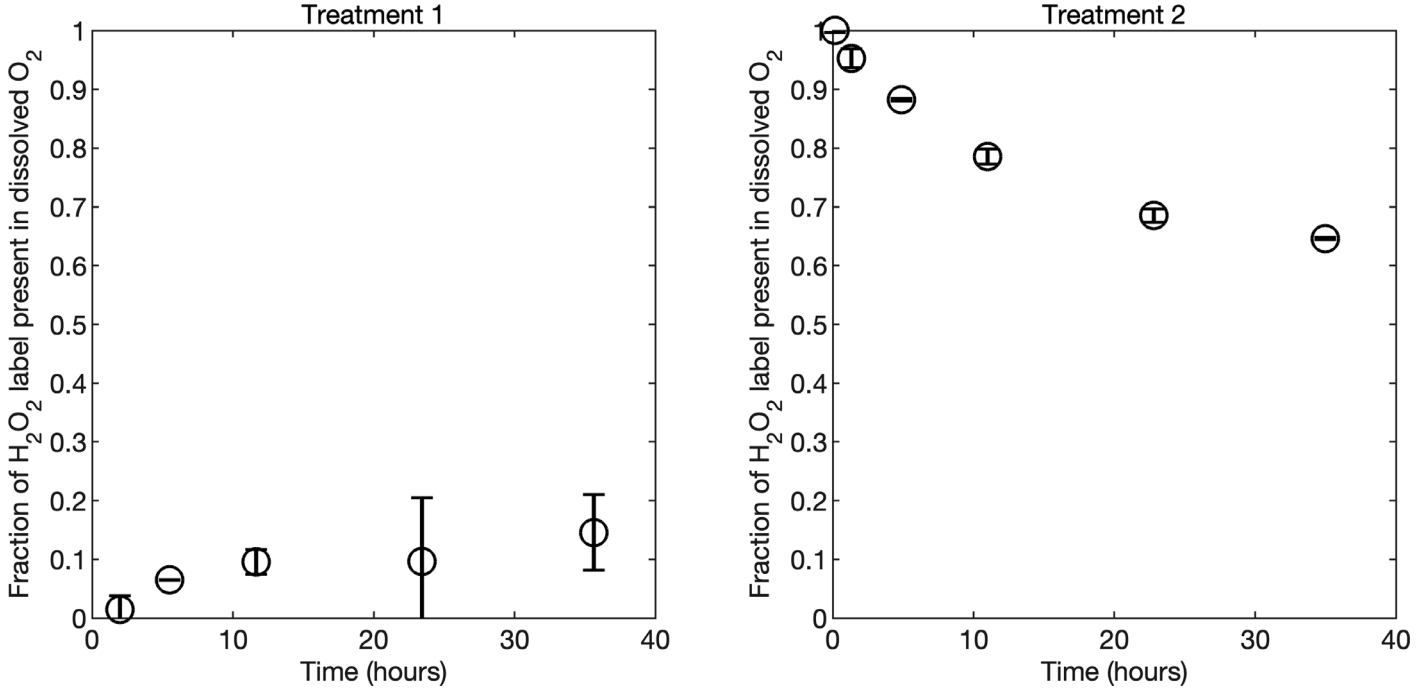

Fig 2. Example of data collected in this study used to determine oxidation, reduction, and gross decay rate constants. Treatment 1 (left) shows the natural evolution of $H_2^{17}O_2$ label into the dissolved oxygen pool as a function of time. Treatment 2 (right) shows the decrease in the total label following an oxidizing treatment (converting all unreacted H_2O_2 to O_2) as a function of time. These data were used with Eqs. 3–9 to determine the three decay rate constants.

were measured using the POHPPA (4-hydroxyphenylacetic acid) technique, as previously described elsewhere (Miller and Kester 1988; Miller et al. 2005; Shaked and Armoza-Zvuloni 2013). In summary, horseradish peroxidase catalyzes the reaction between POHPPA reagent and H_2O_2 to form a fluorescent dimer. The POHPPA reagent was prepared with 0.25 mM POHPPA reagent, 70 units mL^{-1} of horseradish peroxidase, and 0.25 M Tris buffer (pH 8.8). The reagent was added to water samples in a ratio of 1 : 50 (reagent : sample), and incubated in dark amber vials for a minimum of 10 min before its fluorescence spectrum was collected. Fluorescence was measured using a Molecular Devices SpectraMax M3 with excitation at 315 nm and emission at 408 nm. Standard curves were prepared each day by adding H_2O_2 (3% H_2O_2 w/w, Sigma) to filtered seawater, and separate standard curves were prepared for photic and aphotic depths. H_2O_2 stock solutions were quantified each day from ultraviolet (UV) absorbance at 240 nm before preparing standard curve solutions, typically ranging from 10 nM to 1 μM H_2O_2 (Shaked and Armoza-Zvuloni 2013). The blank was determined by measuring sample fluorescence following the addition of catalase (Sigma, 25 units mL^{-1}). We note that this method cannot distinguish between H_2O_2 and organic peroxide present in the water column (O'Sullivan et al. 2005).

Results

Sta. 1

Sta. 1, the deepest of the three stations, had a mixed layer depth of approximately 20 m. The highest oxygen concentration, approximately 255 μmol kg^{-1}, was measured in the mixed layer (Supporting Information Fig. S1). Below the mixed layer, oxygen concentrations steadily decreased to a minimum concentration of 10 μmol kg^{-1} at approximately 700 m depth, and steadily increased with depth below 700 m to near 100 μmol kg^{-1} at 3000 m depth. Temperature at the surface was approximately 15°C and decreased with depth to approximately 1.7°C in the underlying deep water. CTD-measured chlorophyll-based fluorescence was between 5 and 7 mg m^{-3} in the mixed layer before falling off sharply at the thermocline (Supporting Information Fig. S1).

H_2O_2 gross decay rate constants (k_{loss}, Eq. 9) ranged from 0.0019 to 0.025 h^{-1}, with the highest values in the shallowest depths (Fig. 3; Table 1). The two shallowest depths (both in the mixed layer) exhibited similarly high decay rates, which dropped off by about an order of magnitude below the mixed layer. The oxidation–reduction ratio (k_{ox}/k_{red}) exhibited some variability. The oxidation–reduction ratios in the mixed layer were 1.0 and 0.6 at 4 and 20 m, respectively (Fig. 4; Table 1). At 250 m, oxidation far exceeded reduction by a factor of 2.7. The remaining three depths exhibited oxidation–reduction ratios of 1.0 (750 m), 0.7 (1800 m), and 0.5 (3000 m).

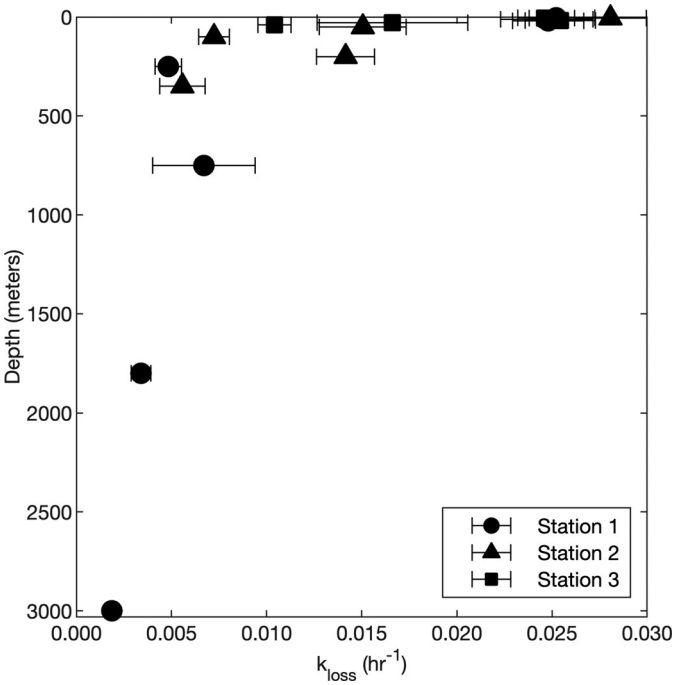

Fig 3. Summary of gross H_2O_2 decay rate constant as a function of water depth at Stas. 1–3.

Sta. 2

At Sta. 2, the water column overlying the Santa Barbara Basin, the mixed layer extended to approximately 20 m depth. Surface dissolved oxygen decreased from ~200 to ~25 μmol kg^{-1} at 350 m, the deepest depth sampled at this site (Supporting Information Fig. S2). Chlorophyll-based fluorescence reached a maximum of 1.8 mg m^{-3} at 12 m depth before decreasing significantly below 22 m. Similar to Sta. 1, surface temperature at Sta. 2 was near 15°C, and decreased to near 8°C at 350 m depth (Supporting Information Fig. S2).

Gross decay rate constants (k_{loss}) for H_2O_2 ranged from 0.0056 to 0.028 h^{-1} (Fig. 3; Table 1), with the highest values present in the surface water. The gross decay rate constants generally decreased with depth, with the exception of the sample collected at 200 m depth, which exhibited a higher rate than the samples above and below it. The overall structure of the oxidation–reduction ratio with depth was very similar to that from Sta. 1, but more compressed in space. The oxidation–reduction ratios at 5 and 50 m were 1.5 and 1.0, respectively (Fig. 4; Table 1). At 100 m, the oxidation rate exceeded the reduction rate approximately threefold. In the bottom two depths, oxidation lagged reduction with oxidation–reduction ratios of 0.4 at both 200 and 350 m.

Sta. 3

Sta. 3, which was just offshore of Catalina Island, California, was included to give a higher-resolution look at H_2O_2 dynamics in the surface ocean. The mixed layer at this site was only

Table 1. Oxidation decay rate constants, reduction decay rate constants, gross decay rate constants, and oxidation–reduction ratio for Stas. 1–3.

Station	Depth (meters)	k_{ox} (h^{-1})	k_{red} (h^{-1})	k_{loss} (h^{-1})	k_{ox}/k_{red}
1	4	0.0128 ± 0.0020	0.0125 ± 0.0005	0.0252 ± 0.0020	1.02 ± 0.16
	20	0.0097 ± 0.0017	0.0151 ± 0.0007	0.0248 ± 0.0019	0.64 ± 0.12
	250	0.0035 ± 0.0007	0.0013 ± 0.0001	0.0048 ± 0.0007	2.75 ± 0.57
	750	0.0033 ± 0.0005	0.0034 ± 0.0027	0.0067 ± 0.0027	0.99 ± 0.79
	1800	0.0014 ± 0.0002	0.0020 ± 0.0005	0.0034 ± 0.0005	0.69 ± 0.18
	3000	0.0006 ± 0.0001	0.0012 ± 0.0003	0.0019 ± 0.0003	0.50 ± 0.17
2	5	0.0167 ± 0.0018	0.0114 ± 0.0007	0.0281 ± 0.0019	1.46 ± 0.18
	50	0.0073 ± 0.0018	0.0077 ± 0.0014	0.0151 ± 0.0023	0.95 ± 0.29
	100	0.0054 ± 0.0008	0.0018 ± 0.0002	0.0072 ± 0.0008	2.94 ± 0.51
	200	0.0043 ± 0.0009	0.0098 ± 0.0012	0.0141 ± 0.0015	0.44 ± 0.11
	350	0.0015 ± 0.0010	0.0041 ± 0.0007	0.0056 ± 0.0012	0.35 ± 0.24
3	5	0.0146 ± 0.0007	0.0100 ± 0.0004	0.0246 ± 0.0008	1.45 ± 0.09
	12	0.0139 ± 0.0022	0.0108 ± 0.0011	0.0247 ± 0.0024	1.29 ± 0.24
	18	0.0127 ± 0.0018	0.0127 ± 0.0005	0.0254 ± 0.0019	1.00 ± 0.15
	28	0.0092 ± 0.0039	0.0074 ± 0.0006	0.0166 ± 0.0040	1.23 ± 0.54
	40	0.0044 ± 0.0006	0.0060 ± 0.0006	0.0104 ± 0.0009	0.74 ± 0.13

10 m deep. Temperature ranged from 19°C in the surface to 12°C at the deepest sampled depth (Supporting Information Fig. S3). Dissolved oxygen exhibited a significant gradient over the 40 m sample depth, with surface water having a concentration of approximately 220 μmol kg^{-1}, increasing to a maximum of 240 μmol kg^{-1} at 15 m, then steadily decreasing to 180 μmol kg^{-1} at 40 m. Fluorescence-based chlorophyll was exceptionally high throughout the sampling depths, ranging between 20 and 23 mg m^{-3}.

Gross H_2O_2 decay rate constants (k_{loss}) at Sta. 3 ranged from 0.010 to 0.025 h^{-1} (Fig. 3; Table 1). The oxidation–reduction ratio of H_2O_2 ranged from 1.5 to 0.7 (Fig. 4; Table 1), with the highest ratio occurring in the shallowest depth (5 m), and the lowest ratio occurring at the deepest depth (40 m). All intermediate depths had oxidation–reduction ratios that fell between these two extremes.

Discussion

The gross decay rate constants of H_2O_2, which ranged from 0.0019 to 0.028 h^{-1}, fall in overlapping ranges with other previously reported values from the marine water column (Figs. 3 and 5). The highest surface value reported here ($\sim$ 0.028 h^{-1}) are actually quite modest in comparison to a handful of other studies that observed surface H_2O_2 decay rate constants in excess of 0.1 h^{-1} (Fig. 5) (Moore et al. 1993; Herut et al. 1998; Vermilyea et al. 2010). Gross decay rate constants fall off significantly below the surface ocean (Fig. 3). The deep ocean (> 1000 m) gross decay rate constants ranged from 0.0019–0.0034 h^{-1}, which were all collected at Sta. 1 (Table 1). These deep ocean gross decay rate constants were lower than any other decay rate constant that we identified in the literature, a point that underscores the fidelity of the sampling methods outlined above. As microbes are the primary sink of H_2O_2 in the ocean, it is not unexpected that gross H_2O_2 decay rate constants mirror typical cell abundance in the water column (Whitman et al. 1998; Steinberg et al. 2001).

The oxidation–reduction ratio at the three stations varied significantly across all sites and depths with a range of 0.4–2.9 (Fig. 4). This range narrows significantly (0.4–1.5) if we omit the two depths with markedly elevated oxidation rates. To our knowledge, only one previous study has investigated the redox fate of H_2O_2 in the marine water column. Using similar isotopic methods, that study found that the surface water (i.e., collected at $\sim$ 0 m depth) in Vineyard Sound (off the coast of Massachusetts) exhibited H_2O_2 decay that was 65% to 80% catalase-like with the remainder being peroxidase-like (Moffett and Zafiriou 1990). This corresponds to an oxidation–reduction ratio of 0.4–0.7. While we observed one depth with an oxidation–reduction ratio in the photic zone that was in this range (0.6, Sta. 1, 20 m), the shallowest depths at the three stations exhibited oxidation–reduction rations ranging from 1 to 1.5 (Fig. 4). These findings underscore significant heterogeneity in the ultimate redox fate of H_2O_2 within the surface ocean. For a given reduction rate, the oxidation rate can exceed or lag the reduction rate by as much as 50%. In the deep ocean (> 1000 m), both incubations exhibited reduction rates that exceed oxidation rates (oxidation–reduction ratio: 0.5–0.7), suggesting a combination of catalase-like and peroxidase-like decay stoichiometry. While this may be microbially mediated, dissolved organic carbon and dissolved metals liberated

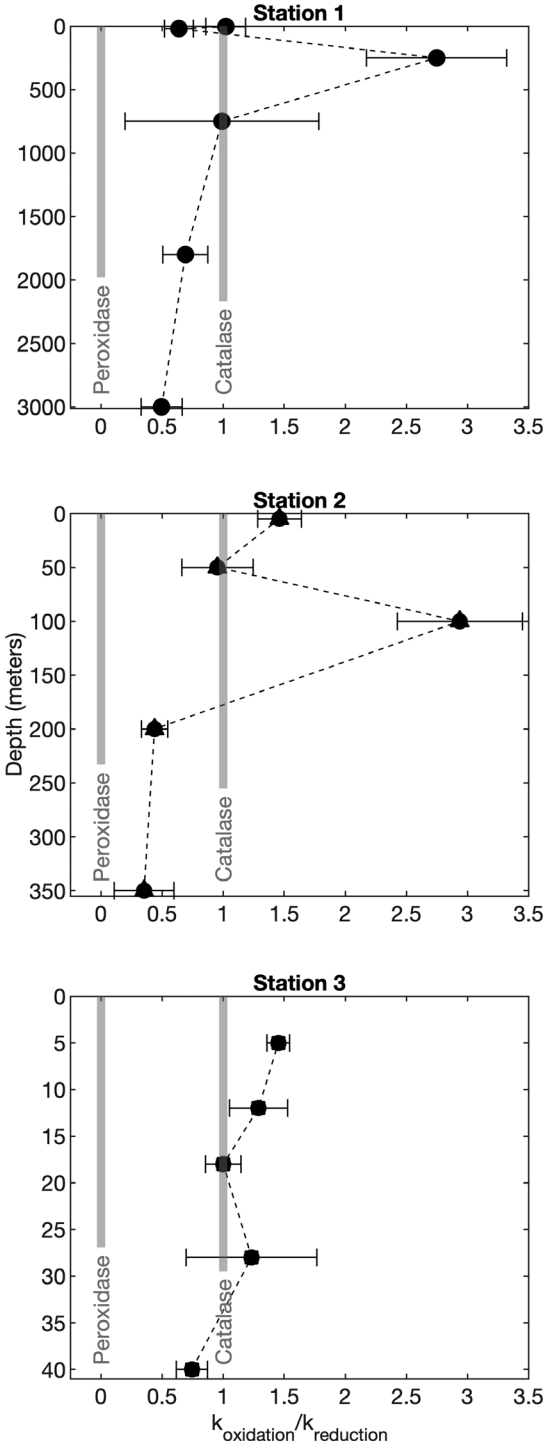

Fig 4. The water column oxidation–reduction ratio (k_{ox}/k_{red}) at Stas. 1–3. Vertical gray reference lines correspond to the oxidation–reduction ratios corresponding to peroxidase and catalase.

during remineralization reacting with H_2O_2 may mimic the stoichiometry of these two general enzyme groups.

One curious feature that we observed in all three sample locations was one or more depths in which oxidation rate exceeded reduction rate. In the case of the shallowest photic depths at all stations, the oxidation to reduction ratio fell between 1 and 1.5. There were also two sub-photic zone sample depths, 250 m depth at Sta. 2 and 100 m depth at Sta. 3, where oxidation far exceeded reduction rate with oxidation–reduction ratios of approximately 3 (2.8 at Sta. 2 and 2.9 at Sta. 3, Fig. 4). Recall that the stoichiometries of H_2O_2 degradation resulting from known enzymatic pathways should fall between oxidation–reduction ratios of 0 and 1 for peroxidase-like and catalase-like decay, respectively. Although there is no known enzymatic H_2O_2 degradation pathway to account for oxidation–reduction ratios that exceed 1, any environmental factors that select for or against organisms lacking a gene for catalase (e.g., *Prochlorococcus*, Thaumarchaeota) can modulate the stoichiometry of the microbial contribution to H_2O_2 degradation (Morris et al. 2011; Hollibaugh 2017). Similarly, H_2O_2 concentrations may play a role in the overall H_2O_2 degradation stoichiometry expressed because of differences in the enzyme kinetics among different catalases, bifunction catalase-peroxidases, and peroxidase. Common dissolved metals like Fe and Mn may also be responsible for H_2O_2 degradation, however, these metals are known to degrade H_2O_2 via disproportionation or reduction (Dole et al. 1952), resulting in the same stoichiometric boundaries as biology. These results suggest that there are strong oxidants in the marine water column that rival, and even exceed direct microbial enzymatic degradation of H_2O_2 in these two depth ranges.

tpOne previous study found that H_2O_2 decomposition in sunlit natural water (and in which microorganisms were removed by filtration) resulted in quantitative oxidation of H_2O_2 to O_2 (Moffett and Zafiriou 1993). This study ruled out the possibility that other ROS (including hydroxyl radical, singlet oxygen, and $O_2^{\bullet -}$) oxidized H_2O_2. Instead, they concluded that unknown, photochemically generated oxidants produced at UV wavelengths were responsible for H_2O_2 oxidation. While the nature of potential photochemically-generated oxidants was not investigated in this study, other potential oxidants may include triplet excited states of dissolved organic matter and/or carbon-centered radicals formed from the cleavage of such dissolved organic matter (Kieber and Blough 1990; Lester et al. 2013). Organic peroxides can also be formed from interactions between light and dissolved organics (O'Sullivan et al. 2005), and can persist at depths beyond which H_2O_2 concentrations typically decline (Sakugawa et al. 2000). Moffett and Zafiriou (1993) also found that photochemical H_2O_2 degradation rates were approximately 5% of production rates, indicating that light-induced H_2O_2 degradation was likely a minor pathway. If we assume that photochemically generated oxidants are responsible for all the photic zone H_2O_2 oxidation that exceeds catalase stoichiometry, we can attribute 1%, 18%, and 19% of gross H_2O_2 degradation to photochemical processes at the shallowest depths of Stas. 1–3, respectively. Water at Sta. 1 was collected well before

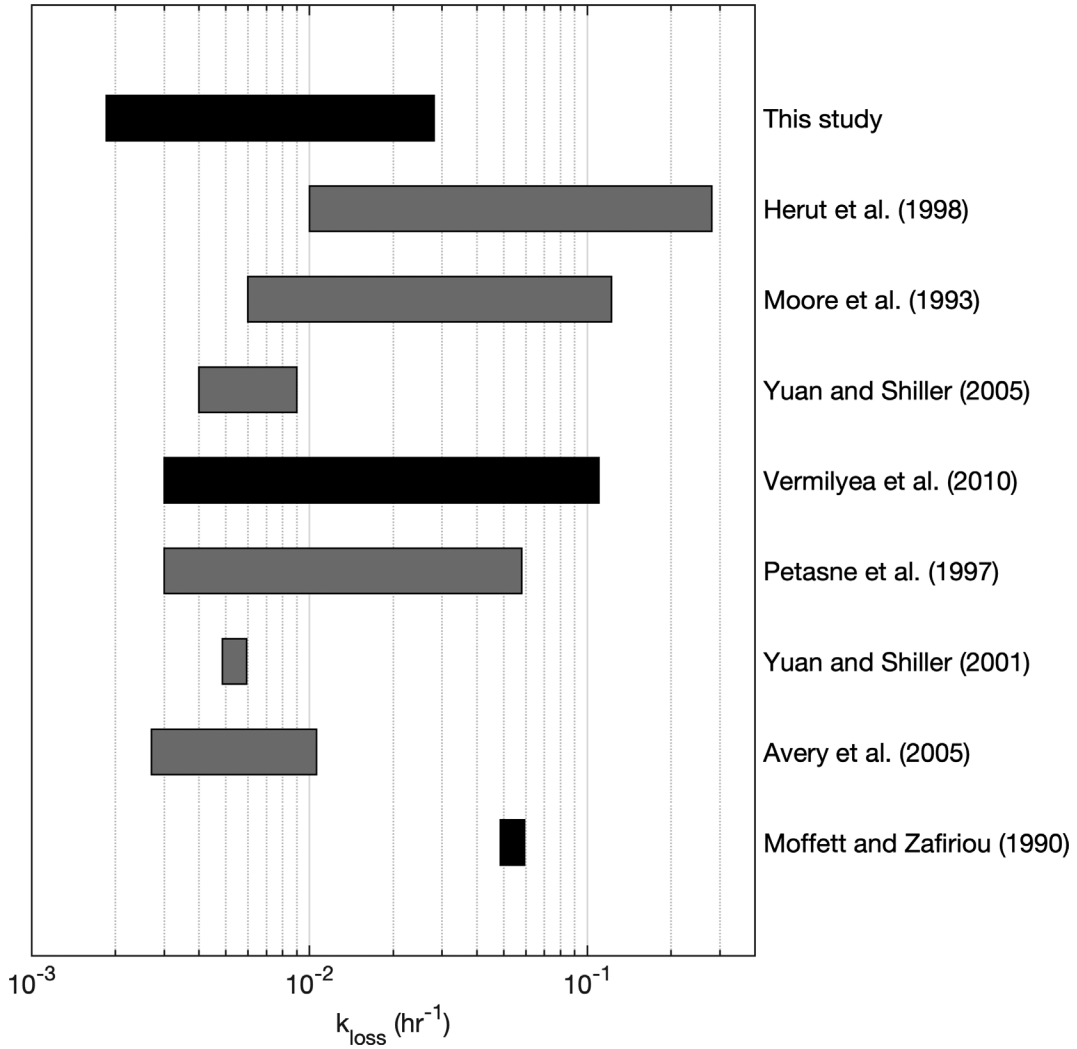

Fig 5. Comparison of first-order decay rate constants for H_2O_2 in seawater, as compiled by Vermilyea et al. (2010). Black bars represent gross decay rate constants, gray bars represent net decay rate constants. Depths of compiled data are as follows: surface (Moffett and Zafiriou 1990), 5–250 m (Avery et al. 2005), surface (Yuan and Shiller 2001), surface—150 m (Petasne and Zika 1997), surface—50 m (Vermilyea et al. 2010), surface (Yuan and Shiller 2005), 2–40 m (Moore et al. 1993), surface (Herut et al. 1998), and 4–3000 m (this study).

sunrise, while water at Stas. 2 and 3 were collected under sunlit conditions and dusk, respectively (see methods), which may explain the large discrepancy. These photochemically generated oxidants likely persist for several hours, but may dissipate after sundown, as evidenced by lower oxidation–reduction ratios in surface waters at Sta. 1.

There remains a need to explain the high relative oxidation rate of H_2O_2 at two sample locations beneath the photic zone. These occur at 250 m depth at Sta. 1 and 100 m depth at Sta. 2 (Fig. 4). Both sample depths are found at intermediate oxygen concentrations between the surface oxygen maxima and intermediate depth oxygen minima. Possible candidates for seawater constituents that could act as oxidants of H_2O_2 with the greatest influence at these depths include nitric oxide (NO) and nitrite (NO_2^-). Both of these nitrogen species typically exhibit maxima in the water column at these depths, and both are produced as a result of ammonium-oxidizing metabolisms beneath the photic zone. While nitrite is the metabolic end product produced by ammonium-oxidizing archaea or bacteria (AOA or AOB), NO is a reactive intermediate formed either by the oxidation of hydroxylamine (Martens-Habbena et al. 2015; Caranto and Lancaster 2017) or the reduction of nitrite by AOA or AOB (Kobayashi et al. 2018). As hypothetical oxidants responsible for H_2O_2 oxidation at these depths, we propose the following reactions:

$$H_2O_2 + 2NO \rightarrow O_2 + N_2O, \quad (10)$$

$$2H_2O_2 + 2NO \rightarrow 2O_2 + N_2, \quad (11)$$

$$2H_2O_2 + 2NO_2^- + 2H^+ \rightarrow 2O_2 + N_2O + 3H_2O, \quad (12)$$

$$3H_2O_2 + 2NO_2^- + 2H^+ \rightarrow 3O_2 + N_2 + 4H_2O, \quad (13)$$

Using a range of natural concentrations for NO and NO_2^- typical of these intermediate aphotic waters (Ward and Zafiriou 1988; Nevison et al. 2003; Ji et al. 2015), we calculated ΔG of reaction under environmental conditions to range from approximately −70 to $-100\,kJ\,mol^{-1}$ when the product was N_2O, and −230 to $-250\,kJ\,mol^{-1}$ when the product was N_2 (assumptions: [NO]: 10–30 pM, $[N_2O]$: 10–25 nM, $[NO_2^-]$: 100–200 nM, $[H_2O_2]$: 500 nM, $[O_2]$: 75 μM, pH: 7.8, $[N_2]$: 600 μM, all thermodynamic parameters taken from Stumm and Morgan 2012) (Stumm and Morgan 2012). Thus, all of these reactions are thermodynamically favored in the forward direction as written, with N_2 being the thermodynamically preferred product over N_2O. Similar reactions may also occur via a peroxynitrite intermediate before ultimately producing the end products written above (Alvarez et al. 1995). If we assume that all H_2O_2 oxidation in excess of catalase stoichiometry was the result of a single unknown oxidant, that oxidant would need to support a H_2O_2 oxidation rate of 27 and 42 nM H_2O_2 per hour (54 and 84 nM equivalents per hour) at Stas. 1 and 2, respectively. There is very little evidence that supports such high N_2O production rates, pointing to N_2 as the most likely product. Given the considerably low standing stock and turnover rate of NO in previous investigations, we suggest NO_2^- as the more likely aphotic oxidant of H_2O_2 (Ward and Zafiriou 1988). Altogether, this makes Eq. 13 the most likely candidate among these four proposed reactions involving nitrogen species. While the incubation concentrations used in this study are quite a bit higher than typical H_2O_2 concentrations in the marine water column, there is circumstantial evidence that NO_x-mediated H_2O_2 oxidation may occur under natural H_2O_2 concentrations. Multiple studies reporting water column H_2O_2 concentrations have observed a local minimum in H_2O_2 concentration at similar depth ranges (Yuan and Shiller 2004; Hopwood et al. 2017). We propose that this may be a direct result of H_2O_2 interactions with nitrite. We note that a previous study demonstrated that increasing H_2O_2 concentrations had an adverse effect on ammonium oxidizers (Tolar et al. 2016). This was evidenced by observing the transformation of isotopically labeled ammonium salt into nitrification products NO_2^- and NO_3^-. However, if our hypothesized interactions between H_2O_2 and NO_2^- ultimately yields N_2, then the adverse effects may be overstated. If N_2 is indeed a result of H_2O_2 oxidation, this reaction may be an unappreciated shunt in the nitrogen cycle that has not yet been explored.

Another group of potential oxidants that can exhibit elevated levels at intermediate water depths include various forms oxidized manganese (Mn) (Jones et al. 2020). Oxidized forms of Mn (Mn(III) and/or Mn(IV)) in the marine water column include Mn(III/IV) oxide particles and Mn(III) ligand-bound complexes (Mn(III)-L) (Oldham et al. 2017). Mn(III/IV) oxide minerals are known to be strong environmental oxidants, and the oxidation of H_2O_2 to O_2 by Mn(IV) oxide has been characterized (Broughton and Wentworth 1947). There is growing recognition that Mn(III)-L complexes can make up a significant fraction of total Mn in the marine water column (Madison et al. 2013; Oldham et al. 2017; Jones et al. 2020). One study of Mn speciation in the North Atlantic found that Mn(III)-L complexes can comprise as much as 45% of the total water column Mn (Jones et al. 2020). Lack of precise thermodynamic data of Mn(III)-L make the potential redox interactions between Mn(III) and H_2O_2 difficult to predict, however there is evidence that ligand-bound Mn(III) can oxidize H_2O_2 directly to O_2 (Jones and Hamm 1974). The identity of Mn(III)-binding ligand(s) is an active area of research; humic substances and pyrophosphate are two examples of ligands that have been implicated in various marine settings (Oldham et al. 2017; Dijkstra et al. 2018). Dissolved Mn concentrations typically range from < 1 to 10 nM in the open ocean to > 100 nM in near shore environments (Oldham et al. 2020). Manganese can also exhibit dynamic redox behavior over the course of the a day (Oldham et al. 2020). Recall from the previous section that the hypothetical H_2O_2 oxidant would need to support H_2O_2 oxidation rates of 27–42 nM h^{-1}. If Mn oxides or Mn(III)-L complexes are involved in H_2O_2 oxidation, the Mn reservoir would need to be re-oxidized or replaced several times over the course of a day to support this reaction.

Beyond N- and Mn-species, CDOM, copper, iron, and iodide have also been implicated in the catalytic decomposition of ROS including superoxide and H_2O_2 (Moffett and Zika 1987; Goldstone and Voelker 2000; Wong and Zhang 2008). While these reactions typically yield disproportionation stoichiometry (i.e., catalase-like stoichiometry), specific circumstances including an oxidized reactant pool or co-occurrence of multiple of these redox-active species with H_2O_2 could also theoretically yield net oxidation of H_2O_2.

While the mechanisms that underlie oxidative and reductive H_2O_2 loss need to be further evaluated, we can use the data collected in this study to draw some quantitative conclusions as to the typical redox fate of H_2O_2 in the marine water column. Using linear interpolation between depths, and weighting the redox fate at each depth by the gross decay rate at that depth, we find that the depth-integrated oxidation–reduction ratios of H_2O_2 are 0.93, 0.96, and 1.2 for Stas. 1–3, respectively. As noted above, we observed two depths with significantly elevated H_2O_2 oxidation rates in intermediate waters that may be related to interactions with an unknown oxidant. If this is the case, it is likely that the depth ranges of elevated H_2O_2 oxidation relative to H_2O_2 reduction are much more limited than would be expected from linear interpolation between depths. If we omit these two depths from Stas. 1 and 2, we find that the depth-integrated oxidation–reduction ratio of H_2O_2 is then 0.74, 0.67, and 1.2 for Stas. 1–3, respectively. Two important aspects that this calculation is not able to capture are the H_2O_2 production rate and steady-state concentration. Steady-state H_2O_2 concentrations and production rates are typically 1–2 orders of magnitude higher in surface water than in deep waters, resulting from both photochemical and biological activity (Hopwood et al. 2017).

Weighting the depth-integrated redox fate by production rate would increase the weight of surface depths on the overall oxidation–reduction ratio. At Stas. 1 and 2, this would likely increase the integrated oxidation–reduction ratio slightly. The depth-integrated estimate for the fate of H_2O_2 at Sta. 3, an oxidation–reduction ratio of 1.2, is likely the most representative of the environment since the production rate range over the surface depths is certainty smaller than at Stas. 1 and 2. The notable difference between the integrated oxidation–reduction ratio we determined at Sta. 3 and that presented in Moffett and Zafiriou (1990) (1.2 in this study vs. 0.4–0.7 in Moffett and Zafiriou) hints at some larger underlying biogeochemical controls on the fate of H_2O_2 that are not fully resolved in either study. Spatiotemporal variations in H_2O_2 degradation stoichiometry may be explained by varying contributions of photochemical products, the identity and redox state of redox active species, and the size, identity, and gene expression of a water parcel's microbial constituents. Future work should target the dynamic range of the H_2O_2 oxidation–reduction ratio in the surface ocean over an entire 24-h light cycle, the seawater chemistry and microbial assemblages that underlie different decay regimes, and the nature of non-enzymatic H_2O_2 oxidation in surface and intermediate waters.

Summary and conclusion

We used an isotope labeling approach to measure the gross oxidation, reduction, and total loss rate constants of H_2O_2 at three distinct water column environments in the Eastern Pacific off the coast of California. In general, the gross H_2O_2 decay rate constant decreased with increasing depth. The oxidation to reduction ratio exhibited significant variability with depth. While we hypothesized that H_2O_2 decay would be governed primarily by peroxidase-like and catalase-like dynamics, measured decay stoichiometry violated this assumption at several depths in the water column. In the photic zone and intermediate depth waters, gross oxidation rates exceeded gross reduction rates by as much as a factor of 3. This excess oxidation in the photic zone likely results from photochemically generated radicals that are stable on the order of several hours. Excess oxidation at intermediate depths may be linked to reactions with other oxidants, including nitrification products NO or NO_2^-; however, this relationship needs to be verified. The depth-integrated H_2O_2 oxidation–reduction ratio ranged from 0.7 to 1.2 depending on the particular station and assumptions used.

ROS production and cycling in the marine environment represents a significant flux and potential sink of marine dissolved oxygen. H_2O_2 production and degradation resulting from photochemical and biological processes is a critical component of this flux. The overall redox fate of H_2O_2 in the surface ocean has the largest influence on whether net O_2 reduction or cryptic O_2 recycling will result from H_2O_2 formation in the marine water column. We found that a slight majority of H_2O_2 in the surface ocean undergoes oxidative decay, a finding that is at odds with the only previous study to investigate the redox fate of this ROS. Beyond the implications of H_2O_2 degradation on dissolved O_2, the redox fate of H_2O_2 is also important for understanding how ROS interacts with other biologically relevant element cycles such as carbon and redox-active metals. In particular, the decay rate constant and redox fate of H_2O_2 will influence the steady state concentrations of H_2O_2, thus controlling the extent to which H_2O_2 can react directly with dissolved constituents of seawater (influencing their bioavailability) and the rate of formation of hydroxyl radical, a potent oxidant of organic carbon. Altogether, our findings suggests that H_2O_2 degradation exhibits spatiotemporal variability, and the extent to which H_2O_2 interacts with dissolved oxygen, dissolved organic carbon, or redox active metals is similarly variable. Clearly, more work is needed to better constrain the biogeochemical controls on H_2O_2 degradation and its ultimate feedbacks on other element cycles.

References

Alvarez, B., A. Denicola, and R. Radi. 1995. Reaction between peroxynitrite and hydrogen peroxide: Formation of oxygen and slowing of peroxynitrite decomposition. Chem. Res. Toxicol. **8**: 859–864.

Avery, G. B., Jr., W. J. Cooper, R. J. Kieber, and J. D. Willey. 2005. Hydrogen peroxide at the Bermuda Atlantic time series station: Temporal variability of seawater hydrogen peroxide. Mar. Chem. **97**: 236–244.

Bender, M., T. Sowers, and L. Labeyrie. 1994. The Dole effect and its variations during the last 130,000 years as measured in the Vostok ice core. Global Biogeochem. Cycl. **8**: 363–376. doi:10.1029/94gb00724

Bograd, S. J., F. B. Schwing, C. G. Castro, and D. A. Timothy. 2002. Bottom water renewal in the Santa Barbara Basin. J. Geophys. Res. Ocean. **107**: 9–9-9. doi:https://doi.org/10.1029/2001JC001291

Broughton, D. B., and R. L. Wentworth. 1947. Mechanism of decomposition of hydrogen peroxide solutions with manganese dioxide. I. J. Am. Chem. Soc. **69**: 741–744. doi:10.1021/ja01196a003

Caranto, J. D., and K. M. Lancaster. 2017. Nitric oxide is an obligate bacterial nitrification intermediate produced by hydroxylamine oxidoreductase. Proc. Natl. Acad. Sci. **114**: 8217–8222. doi:10.1073/pnas.1704504114

Cooper, W. J., and R. G. Zepp. 1990. Hydrogen peroxide decay in waters with suspended soils: Evidence for biologically mediated processes. Can. J. Fish. Aquat. Sci. **47**: 888–893.

Dijkstra, N., P. Kraal, M. J. M. Séguret, M. R. Flores, S. Gonzalez, M. J. A. Rijkenberg, and C. P. Slomp. 2018. Phosphorus dynamics in and below the redoxcline in the Black Sea and implications for phosphorus burial. Geochim.

Cosmochim. Acta **222**: 685–703. doi:https://doi.org/10.1016/j.gca.2017.11.016

Dole, M., D. P. Rudd, G. R. Muchow, and C. Comte. 1952. Isotopic composition of oxygen in the catalytic decomposition of hydrogen peroxide. J. Chem. Phys. **20**: 961–968.

Fridovich, I. 1998. Oxygen toxicity: A radical explanation. J. Exp. Biol. **201**: 1203–1209.

Goldstone, J. V., and B. M. Voelker. 2000. Chemistry of superoxide radical in seawater: CDOM associated sink of superoxide in coastal waters. **34**: 1043–1048. doi:10.1021/es9905445

Guy, R. D., M. L. Fogel, and J. A. Berry. 1993. Photosynthetic fractionation of the stable isotopes of oxygen and carbon. Plant Physiol. **101**: 37–47. doi:10.1104/pp.101.1.37

Hansel, C. M., and J. M. Diaz. 2021. Production of extracellular reactive oxygen species by marine biota. Ann. Rev. Mar. Sci. **13**: 177–200. doi:10.1146/annurev-marine-041320-102550

Helman, Y. 2005. Fractionation of the three stable oxygen isotopes by oxygen-producing and oxygen-consuming reactions in photosynthetic organisms. Plant Physiol. **138**: 2292–2298. doi:10.1104/pp.105.063768

Herut, B., E. Shoham-Frider, N. Kress, U. Fiedler, and D. L. Angel. 1998. Hydrogen peroxide production rates in clean and polluted coastal marine waters of the Mediterranean, Red and Baltic Seas. Mar. Pollut. Bull. **36**: 994–1003. doi:https://doi.org/10.1016/S0025-326X(98)80004-0

Hollibaugh, J. T. 2017. Oxygen and the activity and distribution of marine Thaumarchaeota. Environ. Microbiol. Rep. **9**: 186–188. doi:https://doi.org/10.1111/1758-2229.12534

Hopwood, M. J., I. Rapp, C. Schlosser, and E. P. Achterberg. 2017. Hydrogen peroxide in deep waters from the Mediterranean Sea, South Atlantic and South Pacific Oceans. Sci. Rep. **7**: 43436.

Ji, Q., A. R. Babbin, A. Jayakumar, S. Oleynik, and B. B. Ward. 2015. Nitrous oxide production by nitrification and denitrification in the Eastern Tropical South Pacific oxygen minimum zone. Geophys. Res. Lett. **42**: 10710–755764. doi:https://doi.org/10.1002/2015GL066853

Jones, M. R., G. W. Luther, and B. M. Tebo. 2020. Distribution and concentration of soluble manganese(II), soluble reactive Mn(III)-L, and particulate MnO2 in the Northwest Atlantic Ocean. Mar. Chem. **226**: 103858. doi:https://doi.org/10.1016/j.marchem.2020.103858

Jones, T. E., and R. E. Hamm. 1974. Kinetics of the reaction between 1,2-diaminocyclohexanetetraacetatomanganate (III) ion and hydrogen peroxide. Inorg. Chem. **13**: 1940–1943.

Kana, T. M. 1993. Rapid oxygen cycling in *Trichodesmium thiebautii*. Limnol. Oceanogr. **38**: 18–24.

Kieber, D. J., and N. V. Blough. 1990. Determination of carbon-centered radicals in aqueous solution by liquid chromatography with fluorescence detection. Anal. Chem. **62**: 2275–2283.

Kobayashi, S., and others. 2018. Nitric oxide production from nitrite reduction and hydroxylamine oxidation by copper-containing dissimilatory nitrite reductase (NirK) from the aerobic ammonia-oxidizing Archaeon, *Nitrososphaera viennensis*. Microbes Environ. **33**: 428–434. doi:10.1264/jsme2.ME18058

Kuwabara, J. S., A. van Geen, D. C. McCorkle, and J. M. Bernhard. 1999. Dissolved sulfide distributions in the water column and sediment pore waters of the Santa Barbara Basin. Geochim. Cosmochim. Acta **63**: 2199–2209. doi:https://doi.org/10.1016/S0016-7037(99)00084-8

Lennicke, C., J. Rahn, R. Lichtenfels, L. A. Wessjohann, and B. Seliger. 2015. Hydrogen peroxide—Production, fate and role in redox signaling of tumor cells. Cell Commun. Signal **13**: 39. doi:10.1186/s12964-015-0118-6

Lester, Y., C. M. Sharpless, H. Mamane, and K. G. Linden. 2013. Production of photo-oxidants by dissolved organic matter during UV water treatment. Environ. Sci. Technol. **47**: 11726–11733. doi:10.1021/es402879x

Long, M. H., K. Sutherland, S. D. Wankel, D. J. Burdige, and R. C. Zimmerman. 2020. Ebullition of oxygen from seagrasses under supersaturated conditions. Limnol. Oceanogr. **65**: 314–324. doi:10.1002/lno.11299

Madison, A. S., B. M. Tebo, A. Mucci, B. Sundby, and G. W. Luther. 2013. Abundant porewater Mn(III) is a major component of the sedimentary redox system. Science **341**: 875–878. doi:10.1126/science.1241396

Martens-Habbena, W., and others. 2015. The production of nitric oxide by marine ammonia-oxidizing archaea and inhibition of archaeal ammonia oxidation by a nitric oxide scavenger. Environ. Microbiol. **17**: 2261–2274. doi:https://doi.org/10.1111/1462-2920.12677

Mehler, A. H. 1951. Studies on reactions of illuminated chloroplasts: I. Mechanism of the reduction of oxygen and other hill reagents. Arch. Biochem. Biophys. **33**: 65–77.

Miller, G. W., C. A. Morgan, D. J. Kieber, D. W. King, J. A. Snow, B. G. Heikes, K. Mopper, and J. J. Kiddle. 2005. Hydrogen peroxide method intercomparision study in seawater. Mar. Chem. **97**: 4–13.

Miller, W. L., and D. R. Kester. 1988. Hydrogen peroxide measurement in seawater by (p-hydroxyphenyl)acetic acid dimerization. Anal. Chem. **60**: 2711–2715. doi:10.1021/ac00175a014

Moffett, J. W., and R. G. Zika. 1987. Reaction kinetics of hydrogen peroxide with copper and iron in seawater. Environ. Sci. Technol. **21**: 804–810. doi:10.1021/es00162a012

Moffett, J. W., and O. C. Zafiriou. 1990. An investigation ofhydrogen peroxide chemistry in surface waters of Vineyard Sound with H_2 $^{18}O_2$ and $^{18}O_2$. Limnol. Oceanogr. **35**: 1221–1229.

Moffett, J. W., and O. C. Zafiriou. 1993. The photochemical decomposition of hydrogen peroxide in surface waters of the eastern Caribbean and Orinoco River. J. Geophys. Res. Ocean. **98**: 2307–2313. doi:10.1029/92JC02768

Moore, C. A., C. T. Farmer, and R. G. Zika. 1993. Influence of the Orinoco River on hydrogen peroxide distribution and production in the eastern Caribbean. J. Geophys. Res. Ocean. **98**: 2289–2298. doi:10.1029/92JC02767

Morris, J. J., Z. I. Johnson, M. J. Szul, M. Keller, and E. R. Zinser. 2011. Dependence of the cyanobacterium Prochlorococcus on hydrogen peroxide scavenging microbes for growth at the ocean's surface. PLoS One **6**: e16805.

Nevison, C., J. H. Butler, and J. W. Elkins. 2003. Global distribution of N_2O and the ΔN_2O-AOU yield in the subsurface ocean. Global Biogeochem. Cycles **17**: 1119. doi:https://doi.org/10.1029/2003GB002068

O'Sullivan, D. W., P. J. Neale, R. B. Coffin, T. J. Boyd, and C. L. Osburn. 2005. Photochemical production of hydrogen peroxide and methylhydroperoxide in coastal waters. Mar. Chem. **97**: 14–33. doi:https://doi.org/10.1016/j.marchem.2005.04.003

Oldham, E., A. Mucci, B. M. Tebo, and G. W. Luther. 2017. Soluble Mn (III)—L complexes are abundant in oxygenated waters and stabilized by humic ligands. Geochim. Cosmochim. Acta **199**: 238–246. doi:10.1016/j.gca.2016.11.043

Oldham, V. E., C. H. Lamborg, and C. M. Hansel. 2020. The spatial and temporal variability of Mn speciation in the coastal Northwest Atlantic Ocean. J. Geophys. Res. Ocean. **125**: e2019JC015167. doi:10.1029/2019JC015167

Palenik, B., and F. M. M. Morel. 1988. Dark production of H_2O_2 in the Sargasso Sea. Limnol. Oceanogr. **33**: 1606–1611.

Petasne, R. G., and R. G. Zika. 1997. Hydrogen peroxide lifetimes in South Florida coastal and offshore waters. Mar. Chem. **56**: 215–225. doi:10.1016/S0304-4203(96)00072-2

Powers, L. C., L. C. Babcock-adams, J. K. Enright, and W. L. Miller. 2015. Probing the photochemical reactivity of deep ocean refractory carbon (DORC): Lessons from hydrogen peroxide and superoxide kinetics. Mar. Chem. **177**: 306–317. doi:10.1016/j.marchem.2015.06.005

Powers, L. C., and W. L. Miller. 2015. Hydrogen peroxide and superoxide photoproduction in diverse marine waters: A simple proxy for estimating direct CO_2 photochemical fluxes. 7696–7704. doi:10.1002/2015GL065669.Received

Roe, K. L., R. J. Schneider, C. M. Hansel, and B. M. Voelker. 2016. Measurement of dark, particle-generated superoxide and hydrogen peroxide production and decay in the subtropical and temperate North Pacific Ocean. Deep. Res. Part I Oceanogr. Res. Pap. **107**: 59–69. doi:10.1016/j.dsr.2015.10.012

Rose, A. L., E. A. Webb, T. D. Waite, and J. W. Moffett. 2008. Measurement and implications of nonphotochemically generated superoxide in the equatorial Pacific Ocean. Environ. Sci. Technol. **42**: 2387–2393. doi:10.1021/es7024609

Rose, A. L., A. Godrant, A. Godrant, M. Furnas, and T. D. Waite. 2010. Dynamics of nonphotochemical superoxide production in the Great Barrier Reef lagoon. Limnol. Oceanogr. **55**: 1521–1536. doi:10.4319/lo.2010.55.4.1521

Ryter, S. W., H. P. Kim, A. Hoetzel, J. W. Park, K. Nakahira, X. Wang, and A. M. K. Choi. 2007. Mechanisms of cell death in oxidative stress. Antioxid. Redox Signal. **9**: 49–89. doi:10.1089/ars.2007.9.49

Sakugawa, H., A. Takami, H. Kawai, K. Takeda, K. Fujiwara, and S. Hirata. 2000. The occurrence of organic peroxides in seawater, p. 231–240. *In* Dynamics and characterization of marine organic matter. Springer.

Savarino, J., and M. H. Thiemens. 1999. Analytical procedure to determine both $δ$18O and $δ$17O of H2O2 in natural water and first measurements. Atmos. Environ. **33**: 3683–3690.

Shaked, Y., and R. Armoza-Zvuloni. 2013. Dynamics of hydrogen peroxide in a coral reef: Sources and sinks. J. Geophys. Res. Biogeo. **118**: 1793–1801.

Sheng, Y., I. A. Abreu, D. E. Cabelli, M. J. Maroney, A.-F. Miller, M. Teixeira, and J. S. Valentine. 2014. Superoxide dismutases and superoxide reductases. Chem. Rev. **114**: 3854–3918. doi:10.1021/cr4005296

Steinberg, D. K., C. A. Carlson, N. R. Bates, R. J. Johnson, A. F. Michaels, and A. H. Knap. 2001. Overview of the US JGOFS Bermuda Atlantic Time-series Study (BATS): A decade-scale look at ocean biology and biogeochemistry. Deep Sea Res. Part II Top. Stud. Oceanogr. **48**: 1405–1447. doi:https://doi.org/10.1016/S0967-0645(00)00148-X

Stumm, W., and J. J. Morgan. 2012. Aquatic chemistry: Chemical equilibria and rates in natural waters. John Wiley & Sons.

Sutherland, K. M., and others. 2019. Extracellular superoxide production by key microbes in the global ocean. Limnol. Oceanogr. **64**: 2679–2693. doi:10.1002/lno.11247

Sutherland, K. M., K. C. Grabb, J. S. Karolewski, S. Plummer, G. A. Farfan, S. D. Wankel, J. M. Diaz, C. H. Lamborg, and C. M. Hansel. 2020*a*. Spatial heterogeneity in particle-associated, light-independent superoxide production within productive coastal waters. J. Geophys. Res. Ocean. **125**: e2020JC016747. doi:10.1029/2020JC016747

Sutherland, K. M., S. D. Wankel, and C. M. Hansel. 2020*b*. Dark biological superoxide production as a significant flux and sink of marine dissolved oxygen. Proc. Natl. Acad. Sci. **117**: 3433–3439. doi:10.1073/pnas.1912313117

Tolar, B. B., L. C. Powers, W. L. Miller, N. J. Wallsgrove, B. N. Popp, and J. T. Hollibaugh. 2016. Ammonia oxidation in the ocean can be inhibited by nanomolar concentrations of hydrogen peroxide. Front. Mar. Sci. **3**: 237. doi:10.3389/fmars.2016.00237

Vermilyea, A. W., S. Paul Hansard, and B. M. Voelker. 2010. Dark production of hydrogen peroxide in the Gulf of Alaska. Limnol. Oceanogr. **55**: 580–588. doi:10.4319/lo.2010.55.2.0580

Vlasits, J., C. Jakopitsch, M. Schwanninger, P. Holubar, and C. Obinger. 2007. Hydrogen peroxide oxidation by catalase-peroxidase follows a non-scrambling mechanism. FEBS

Lett. **581**: 320–324. doi:https://doi.org/10.1016/j.febslet.2006.12.037

Ward, B. B., and O. C. Zafiriou. 1988. Nitrification and nitric oxide in the oxygen minimum of the eastern tropical North Pacific. Deep Sea Res. Part A. Oceanogr. Res. Pap. **35**: 1127–1142. doi:https://doi.org/10.1016/0198-0149(88)90005-2

Wassenaar, L. I., J. J. Venkiteswaran, S. L. Schiff, and G. Koehler. 2010. Aquatic community metabolism response to municipal effluent inputs in rivers quantified using diel δ18O values of dissolved oxygen. Can. J. Fish. Aquat. Sci. **67**: 1232–1246. doi:10.1139/F10-057

Whitman, W. B., D. C. Coleman, and W. J. Wiebe. 1998. Prokaryotes: The unseen majority. Proc. Natl. Acad. Sci. USA **95**: 6578–6583. doi:10.1073/pnas.95.12.6578

Wong, G. T. F., and L.-S. Zhang. 2008. The kinetics of the reactions between iodide and hydrogen peroxide in seawater. Mar. Chem. **111**: 22–29. doi:https://doi.org/10.1016/j.marchem.2007.04.007

Wuttig, K., M. I. Heller, and P. L. Croot. 2013. Pathways of superoxide (O-2(-)) decay in the Eastern Tropical North Atlantic. Environ. Sci. Technol. **47**: 10249–10256. doi:10.1021/es401658t

Yuan, J., and A. M. Shiller. 2001. The distribution of hydrogen peroxide in the southern and Central Atlantic Ocean. Deep. Res. Part II Top. Stud. Oceanogr. **48**: 2947–2970. doi:10.1016/S0967-0645(01)00026-1

Yuan, J., and A. M. Shiller. 2004. Hydrogen peroxide in deep waters of the North Pacific Ocean. Geophys. Res. Lett. **31**: L01310. doi:10.1029/2003GL018439

Yuan, J., and A. M. Shiller. 2005. Distribution of hydrogen peroxide in the Northwest Pacific Ocean. Geochem. Geophys. Geosyst. **6**: Q09M02. doi:10.1029/2004GC000908

Zamocky, M., P. G. Furtmüller, and C. Obinger. 2008. Evolution of catalases from bacteria to humans. Antioxid. Redox Signal. **10**: 1527–1548. doi:10.1089/ars.2008.2046

Zhang, T., C. M. Hansel, B. M. Voelker, and C. H. Lamborg. 2016. Extensive dark biological production of reactive oxygen species in brackish and freshwater ponds. Environ. Sci. Technol. **50**: 2983–2993. doi:10.1021/acs.est.5b03906

Zhang, Y., R. Del Vecchio, and N. V. Blough. 2012. Investigating the mechanism of hydrogen peroxide photoproduction by humic substances. Environ. Sci. Technol. **46**: 11836–11843.

Acknowledgments

This work was funded by NSF OCE-1736332 and NSF EAR-1826940 to CMH and SDW, NASA Earth and Space Science Fellowship (grant NNX15AR62H to KMS), Agouron Institute Geobiology Postdoctoral Fellowship (KMS), and NSF GRFP 2016230268 (KCG). KMS would like to thank Richard Hutchings at ICON/Berry and Associates for helpful conversations regarding the isotope-labeling portion of this study.

Conflict of Interest

None declared.

Submitted 05 February 2021
Revised 10 August 2021
Accepted 11 August 2021

Associate editor: Lauren Juranek